Continental Shelf Research 37 (2012) 66–78

Contents lists available at SciVerse ScienceDirect

Continental Shelf Research

journal homepage: www.elsevier.com/locate/csr

Modeling transport and deposition of the Mekong River sediment

Zuo Xue [a,*], Ruoying He [a], J.Paul Liu [a], John C. Warner [b]

[a] Department of Marine, Earth and Atmospheric Sciences, North Carolina State University, Raleigh, NC 27695, USA
[b] US Geological Survey, Coastal and Marine Geology Program, Woods Hole Science Center, Woods Hole, MA 02543, USA

ARTICLE INFO

Article history:
Received 31 January 2011
Received in revised form
6 January 2012
Accepted 19 February 2012
Available online 3 March 2012

Keywords:
South China Sea
Mekong River delta
Coupled sediment transport modeling
Sediment budget

ABSTRACT

A Coupled Wave–Ocean–Sediment Transport Model was used to hindcast coastal circulation and fine sediment transport on the Mekong shelf in southeastern Asian in 2005. Comparisons with limited observations showed that the model simulation captured the regional patterns and temporal variability of surface wave, sea level, and suspended sediment concentration reasonably well. Significant seasonality in sediment transport was revealed. In summer, a large amount of fluvial sediments was delivered and deposited near the Mekong River mouth. In the following winter, strong ocean mixing, and coastal current lead to resuspension and southwestward dispersal of a small fraction of previously deposited sediments. Model sensitivity experiments (with reduced physics) were performed to investigate the impact of tides, waves, and remotely forced ambient currents on the transport and dispersal of the fluvial sediment. Strong wave mixing and downwelling-favorable coastal current associated with the more energetic northeast monsoon in the winter season are the main factors controlling the southwestward along-shelf transport.

1. Introduction

The majority of the world's modern deltaic systems began their formations between 7400 and 9500 cal yr BP as a result of decelerating sea-level rise (Stanley and Warne, 1994). Today, approximate half a billion people are living on or near these deltas. Ever increasing human activities, such as extensive damming have reduced sediment flux to the coastal zones. These, along with a rising sea-level have made deltas regions more vulnerable to storm surges and beach erosion problems. Indeed, 85% of the 33 major deltas of the world have experienced severe flooding in the past decade (Syvitski et al., 2005, 2009). Improved understanding of sediment transport dynamics in deltaic systems is therefore much needed for better coastal resource planning and management.

In southeastern Asia, the Mekong River Delta (MRD hereafter) has an area of 49,500 km^2 (Le et al., 2007). Trailing the Amazon and the Ganges-Brahmaputra Deltas, it is the third largest delta plain in the world (Coleman and Roberts, 1989). The Mekong River itself is the largest river in Southeast Asia. It originates in the Tibetan Plateau, running through China, Myanmar, Thailand, Lao PDR, Cambodia, and eventually to the South China Sea (SCS hereafter) in southern Vietnam (Fig. 1a). The river has a length of ~4750 km and a drainage area of 832,000 km^2 (Xue et al., 2010a). Its annual freshwater discharge is $\sim 470 \times 10^9$ m^3 and the estimated annual sediment flux is ~160 million tons (Milliman and Syvitski, 1992). The weather systems in the lower Mekong region are dominated by the Southeast Asian monsoon. Approximately 80% of the annual rainfall happens during the rainy season between May and October (Debenay and Luan, 2006). Because of this, river discharge in the lower Mekong reaches a maximum in September and a minimum in April (see averaged water discharge at Pakse station during 1960–2005 in Fig. 2a). The resulting MRD is bounded by the SCS to the east and the Gulf of Thailand (GOT hereafter, Fig. 1a) to the west. Borehole studies showed that this delta plain began its progradation in 8000 cal yr BP as a result of decelerating sea-level rise (Tamura et al., 2009). Over the past 5500 yrs, tremendous amount of Mekong River sediment input has allowed the MRD to prograde more than 250-km to the southeast (Nguyen et al., 2000). Recent observations on sediment grain size variations along boreholes further suggested the MRD evolution during this period experienced a phase shift from "tide-dominated" to "tide-and-wave-dominated" condition around 3000 BP (Ta et al., 2002a, 2002b). Today, with ~200 new dams to be added to the river basin in the next couple of decades, more significant changes are expected in MRD hydrological regime, coastal circulation, and delta dynamics (Xue et al., 2010a).

Research progresses on quantifying the physical processes in MRD have been hindered by lacking of observations. As a result, the computer modeling approach has been widely used. Earlier circulation modeling studies have shown that the monsoonal wind produces a basin-wide cyclonic gyre in winter and double

* Corresponding author. Tel.: +1 919 515 0389.
E-mail address: zxue@ncsu.edu (Z. Xue).

0278-4343/$ - see front matter © 2012 Elsevier Ltd. All rights reserved.
doi:10.1016/j.csr.2012.02.010

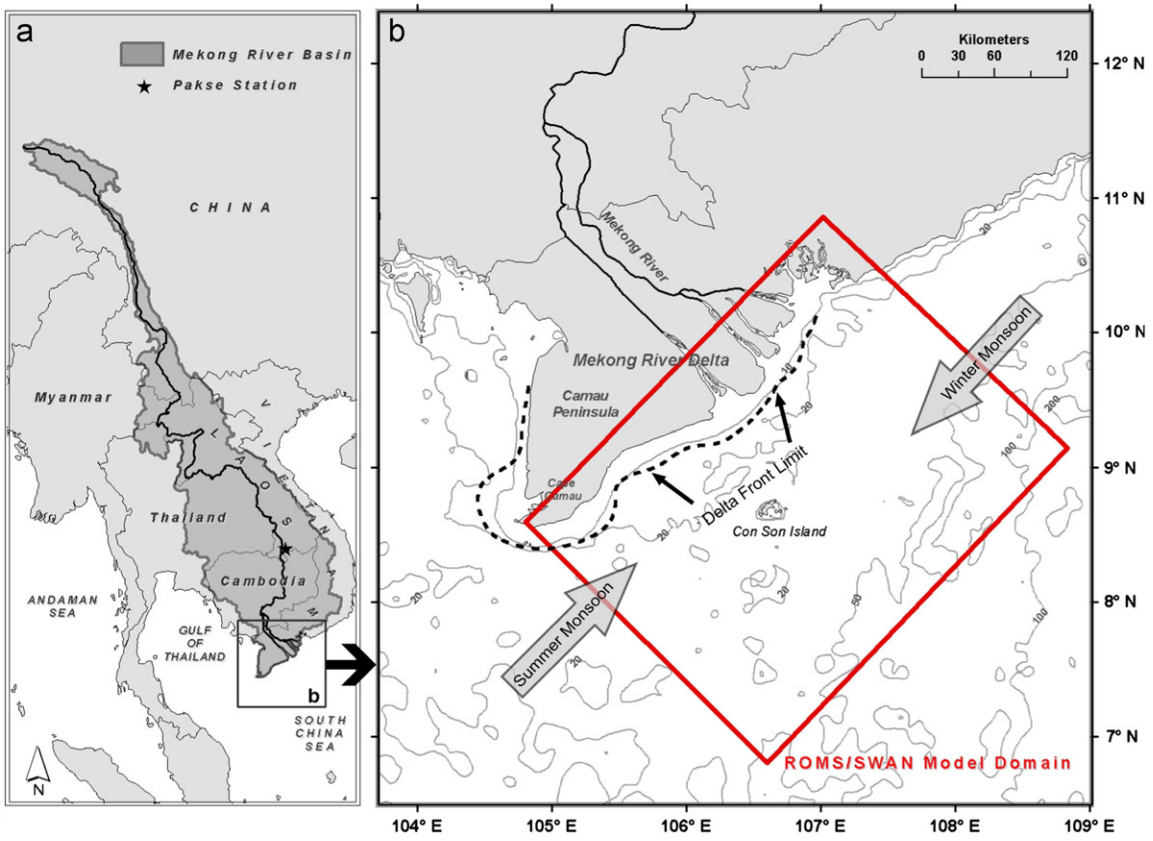

Fig. 1. A map of the Mekong River Delta and the ROMS/SWAN model domain. (a) Mekong River basin with the location of the study area shown by a black box. (b) The ROMS/SWAN model domain used in this study. The positions of delta front limit are from Xue et al. (2010b).

gyres in summer with a cyclonic flow in the north and an anticyclonic flow in the south (Shaw et al., 1999; Liu et al., 2001; Gan et al., 2006; Wang et al., 2006). SW monsoon season runs from May to October and NE monsoon season from November to April (Fig. 3a and b). A recent modeling study by Kubicki (2008) showed the coastal current northwest of the Mekong River mouth has similar directional shifting from NE in winter to SW in summer. Tides are another important circulation process. The amplitude of the dominant semi-diurnal tide M2 (diurnal tide K1) decreases (increases) after the tidal waves propagate from the western Pacific into the SCS through the Luzon Strait (Zu et al., 2008). Both M2 and K1 tidal amplitude are more than 0.9 m seaward of the Mekong River mouth (Fig. 3c and d). Hordoir et al. (2006) simulated the Mekong River plume, indicating that: (1) the large amount of fresh water discharged by the Mekong River forms a baroclinic coastal current flowing in the propagation direction of Kelvin wave; (2) the Mekong River plume is mostly geostrophic and exhibits a strong seasonal variability related to the monsoon wind.

Sedimentary studies of the Mekong Shelf are limited by the scarce of observations as well. Earlier geological studies have focused on MRD long-term (millennium to a couple of thousands years) evolution. A recent acoustic profiling investigation started to reveal some spatial details of the subaqueous deltaic system. For instance, an up to 20-m thick subaqueous delta was identified at the front of the deltaic system (Liu et al., 2009; Xue et al., 2010b). This subaqueous delta accounted for ~80% of the fluvial sediment input over the past 3000 yrs. On a relative shorter time scale; however, significant erosion with a rate of 1.1 km^2/yr, has been documented along the eastern part of the MRD (SCS side) since 1885 (Saito, 2000). While there is a general consensus that the MRD formation is a result of along-shelf sediment transport (Gagliano and McIntire, 1968; Nguyen et al., 2000; Xue et al., 2010b), the Mekong sediment transport dynamics has not been fully quantified. Xue et al. (2010b) based on acoustic profiling and coring data proposed the following seasonal sediment transport/dispersal mechanism: during the high flow season (May–October), a considerable part of riverine sediment was delivered to the Mekong River mouth and temporally deposited there; then during the low flow season (November–April), previously deposited sediment was resuspended by strong mixings associated with the strong northeast monsoon and subsequently transported southwest along-shelf by coastal circulation.

It is worth noting that significant progress in understanding general river sediment transport and dispersal dynamics has been made through the combination of in situ observations (e.g. tripod deployment) and three-dimensional prognostic model simulations. Some recent examples in this regard include a series of river sediment studies conducted in the Adriatic Sea (e.g., Traykovski et al., 2007; Harris et al., 2008; Bever et al., 2009). Numerical modeling is in particular useful in testing mechanism and hypothesis deduced from limited observations, and this is the approach we will utilize in this study as well. Our objectives are two-fold: (1) to better understand the seasonal transport and dispersal patterns of Mekong-derived sediments using a newly developed wave–current–sediment coupled ocean model; and (2) to investigate the relative importance of along-shelf current, waves, and tides in transporting and dispersing Mekong-derived sediments.

2. Methods and data

We applied the Coupled Ocean–Atmosphere–Wave–Sediment Transport Modeling system (COAWST, Warner et al., 2010) in this study to simulate the transport and dispersal of Mekong-derived

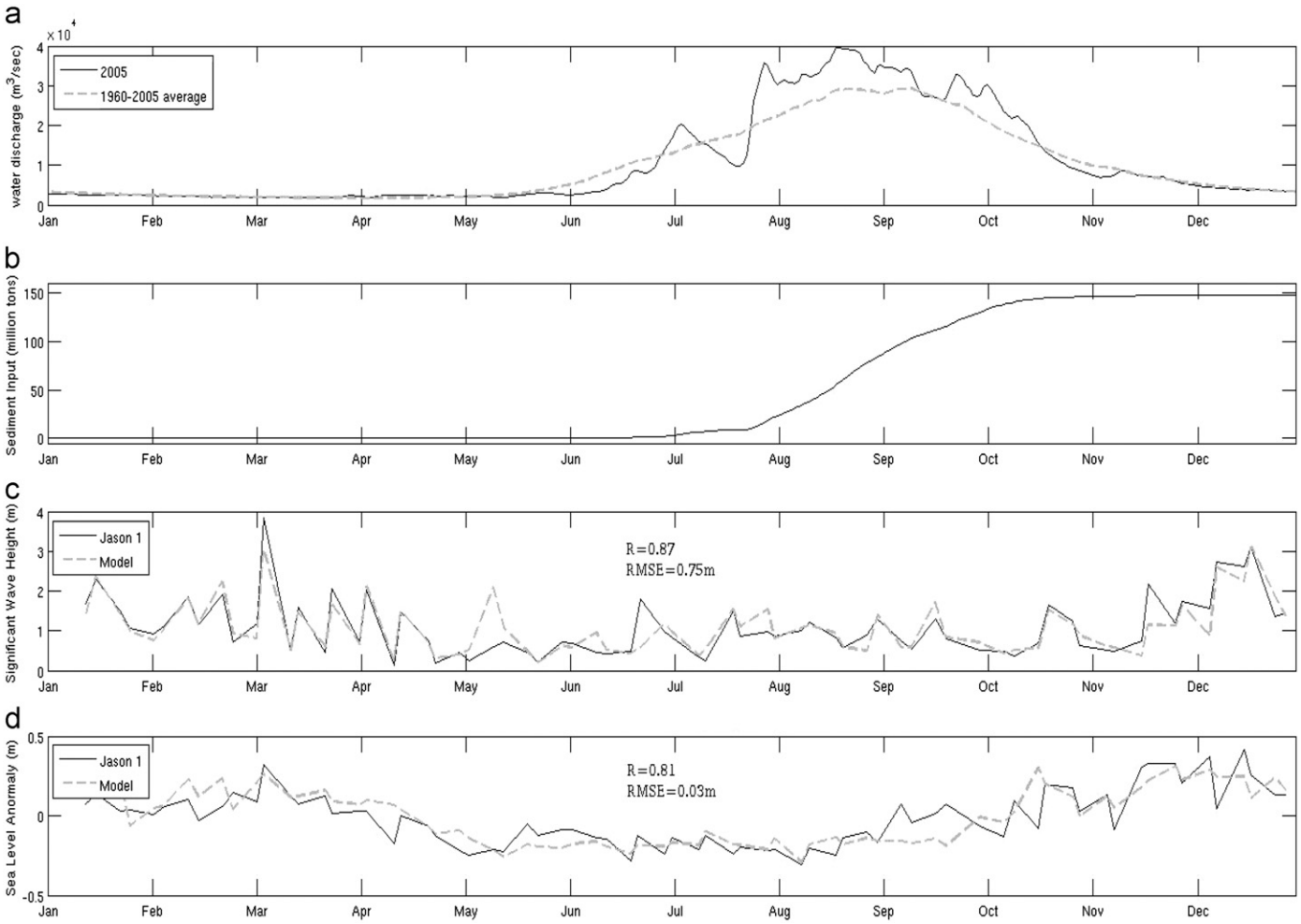

Fig. 2. Time series of (a) water discharge at Pakse station in 2005 (black, solid line) and mean water discharge averaged over 1960–2005 (gray dashed line), (b) the accumulated amount of fluvial sediment input used in the model simulation, (c) comparison between simulated (dashed line) and observed (solid line) significant wave heights. The observed wave heights were measured by Jason-1 altimeter and averaged along satellite tracks within the model domain, and (d) comparison between simulated (dashed line) and observed (solid line) sea-level anomaly. The observed sea-level anomaly was measured by Jason-1 altimeter and averaged along satellite tracks in the model domain.

sediment in 2005. The COAWST system consists of several state-of-the-science modeling components, including ROMS (Regional Ocean Modeling System, Shchepetkin and McWilliams, 2005, 2009; Haidvogel et al., 2008) for the coastal ocean circulation, WRF (Weather Research and Forecasting Model, Skamarock et al., 2005) for regional atmospheric circulation, and SWAN (Simulating Waves Nearshore, Booij et al., 1999) for surface wave. Additionally, the system includes a sediment transport (Community Sediment Transport Modeling System, Warner et al., 2008) module as a part of ROMS, and a model coupler (Model Coupling Toolkit, Larson et al., 2005; Jacob et al., 2005) to exchange data fields. For our research purpose, we disabled atmosphere (WRF) coupling to focus on interactions among ocean–wave–sediment. We note by coupling waves with ocean circulation, the COAWST system accounts for wave-induced enhancement of surface roughness, water column mixing, and bottom stresses (Warner et al., 2010).

Our model domain has 200 × 150 grid points with its lower left boundary corner at 8.6°N and 104.8°E (Fig. 1b). The ocean (ROMS) and wave (SWAN) models have the same computational domain and horizontal resolution of 2 km. The 2-km resolution is smaller than the baroclinic Rossby radius of the regional circulation (Hordoir et al., 2006), allowing the model to represent appropriate dynamical processes in our study region. The 30-s Global Bathymetry and Elevation Data (SRTM30_PLUS, Becker et al., 2009) was smoothed and interpolated to the model grid. Water depths within the computational domain vary from 5.0 to 157.8 m. 20 terrain-following vertical layers was used to resolve water columns. We applied the method of Mellor and Yamada (1982) to compute the vertical turbulent mixing, as well as the quadratic drag formulation for the bottom friction specification.

The circulation model has three open boundaries (northern, eastern, and southern). A one-way nesting approach was used to downscale HYCOM/NCODA (1/12° equatorial resolution, Hybrid Coordinate Ocean Model together with NRL Coupled Ocean Data Assimilation scheme, Chassignet et al., 2007) to the regional ROMS. Specifically, open boundary conditions were applied to ROMS tracers and baroclinic velocity following the method of Marchesiello et al. (2001), whereby Orlanski-type radiation conditions were used in conjunction with relaxation to HyCOM/NCODA solutions. Free surface and depth-averaged velocity boundary conditions were specified using the method of Flather (1976) with the external subtidal information defined by HyCOM/NCODA plus four tidal constituents (S_2, M_2, K_1, O_1) that were derived from the OSU TOPEX/Poseidon Global Inverse Solution 7.0 (Egbert and Erofeeva, 2002). Similarly, the SWAN model wave boundary condition was obtained from the NOAA Wavewatch III (Tolman, 2002) global ocean wave model solutions. The 3-hourly

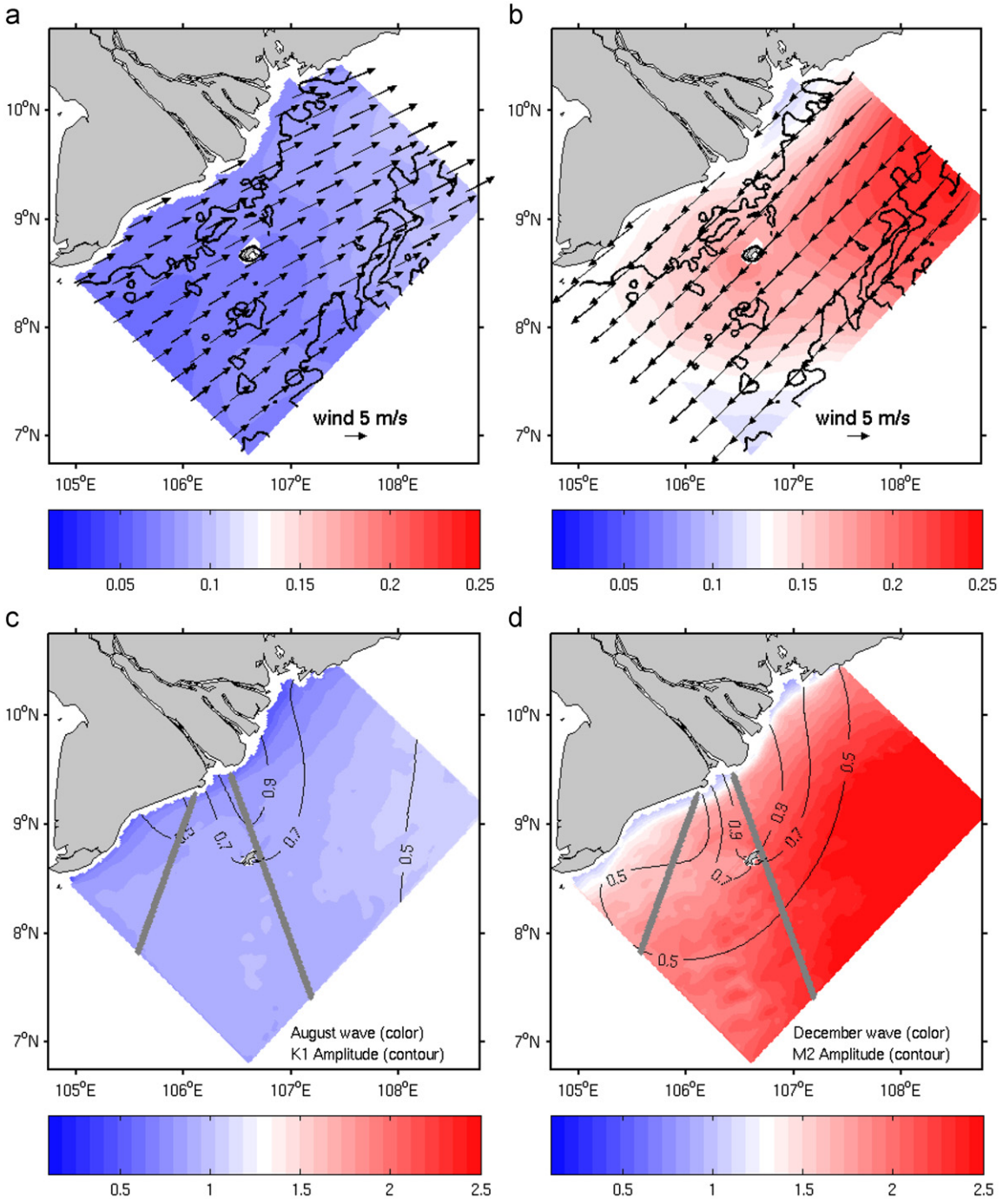

Fig. 3. Monthly mean wind vectors and stress (color shading) and simulated significant wave heights in August and December. Also superimposed on the wave height field (c, d) are the positions of satellite (Jason-1) tracklines (gray color, there are 2300 observational points through 2005) and K1 and M2 tidal amplitude. Surface wind data are taken from QSCAT/NCEP Blended 10-m Ocean Wind product. Tidal amplitude data are taken from OSU TOPEX/Poseidon Global Inverse Solution 7.0. (a) August wind vectors and stress (Pa), (b) December wind vectors and stress (Pa), (c) wave height in August and K1 tide (m) and (d) wave height in December and M2 tide (m). (For interpretation of the references to color in this figure legend, the reader is referred to the web version of this article.)

significant wave height, wave period, and peak direction were all interpolated from 2005 global Wavewatch III model hindcast (1.25° horizontal resolution) along the open boundary of the SWAN model and imposed with a prescribed JONSWAP spectra (Tolman, 2002).

For surface forcing, we used the scheme of Fairall et al. (1996) to compute the surface wind stresses based on the QSCAT/NCEP Blended 10-m wind product (0.5° resolution) generated by Colorado Research Associates. Surface heat fluxes were taken from the global NCEP Reanalysis (2.5° resolution, Kalnay et al., 1996). The temporal resolution of wind stresses and surface heat flux was 3 hourly and daily, respectively.

The sediment transport module consists of algorithms for computing suspended-sediment transport, bed load transport due to current and wave–current forcing, enhanced bottom stress due to surface waves, and a multiple-bed model for tracking stratigraphy, morphology of multiple sediment classes (Warner et al., 2008, 2010). Due to lack of observations of the bulk bed characteristics on the Mekong Shelf, we neglected sandy sediment and shelf sediment in our simulation, and only considered

fine sediment discharged by the Mekong River. Previous observational studies in the Mekong estuary indicated that most of Mekong sediments are flocculated fine particles. During low flow season, observed floc size was 30–40 μm and the clay content was 20–40% by volume (Wolanski et al., 1998). In comparison, during high flow season the floc size was 50–200 μm and the clay content was 20–30% by volume (Wolanski et al., 1996). Based on these, our model only included two classes of sediments: Class 1, accounting for 30% of fluvial sediment input, represents fine materials that travel as slow-settling single grains; Class 2, accounting for 70% of fluvial sediment input, represents flocculated materials. Because in-situ observation of the bulk bed was very limited in this region, we followed the setup in the Po River sediment transport modeling study by Harris et al. (2008) to define sediment hydrodynamic properties. The critical shear stress (τ_{cr}) was set to 0.03 N/m^2 for fine grained material and 0.08 N/m^2 for flocculated material. The settling velocity for fine grained material and flocculated materials were set to be 0.1 mm/s and0.25 mm/s, respectively. The latter value was verified against observations by Wolanski et al. (1998). In the model simulation, the suspended sediment was transported by 3-dimensional shelf circulation. The bottom-boundary layer (BBL) calculation accounts for the interaction of wave and current over a moveable bed (Madsen, 1994; Styles and Glenn, 2000; Wiberg and Harris, 1994; Harris and Wiberg, 2001). Sediment exchange between the bottommost layer of the water column and the seabed occurs at a rate determined by the difference between sediment settling and resuspension. The initial value of suspend sediment concentration (SSC hereafter) was set to be zero over the entire model domain. Along the three open boundaries of the model, a no-gradient boundary condition was applied for sediment tracer.

Fluvial input (water discharge and suspended sediment) from Mekong River was distributed at 65 grid points near the river mouth. The freshwater discharge time series was retrieved from an inland gage station Pakse operated by the Mekong River Commission (see Fig. 1a for station location; Fig. 2a for freshwater discharge time series). In contrast to nearly continuous flow measurement, SSC observations were very sporadic. We therefore adopted the water discharge-SSC rating curve derived by Kummu and Varis (2007, for the same station), which is given by

$$y = 0.00085x^{1.3}$$

where y stands for the total suspended sediment (mg/l) and x the Mekong River discharge rate (m^3/s). Based on this relationship, the total amount of Mekong River sediment input over our 13-months study period (Fig. 2b) was 148.3 million tons, which was comparable to an earlier estimation (160.0 million tons per year) by Milliman and Syvitski (1992).

We began the 13-months model hindcast on December 1st, 2004. Initial hydrodynamic conditions including salinity, temperature, free surface, and current velocities were all taken from HYCOM/NCODA described above. The first month (December 2004) of simulation was used as the model spin-up/adjustment period. Subsequent simulation of sediment transport and dispersal in the whole year of 2005 was used for analysis. We chose 2005 as our case study period based on the following considerations: (1) the weather (e.g., wind and sea level pressure) patterns in 2005 are similar to their long-term mean conditions during 1948–2009, (2) the HyCOM/NCODA database has complete coverage in 2005, and (3) no major typhoon events occurred in the study area. Therefore, we presume the simulated Mekong Shelf circulation and sediment transport/dispersal patterns in 2005 are "typical" representations of the transport processes under the present climatic condition. A 180-s time-step was used in both SWAN and ROMS simulations. Coupled model variables, including the significant wave height, wave length, wave direction, wave periods, bottom orbital velocity, and surface currents were exchanged between SWAN and ROMS on hourly basis.

To investigate the relative importance of ambient shelf current, waves, and tides in transporting and dispersing Mekong-derived sediments, we conducted four sensitivity simulations: Exp 1 (the ***control*** run) considered all aforementioned forcing agents; Compared to Exp 1, Exp 2 excludes tides (***NTS*** hereafter), whereas Exp 3 excludes waves (***NWS*** hereafter). As previously described, the ambient shelf current is controlled by the seasonal shift between NE and SW monsoons. In Exp 4, we consider both waves and tides, but excluded the shelf current (***NAS*** hereafter, i.e. no subtidal circulation forcing at open boundaries) to exam the influence of SCS circulation.

3. Results

Because no in-situ wave and current observations was available on the Mekong Shelf, we used satellite (Jason-1) observations (http://www.aviso.oceanobs.com/duacs/) for model validation. Within each of its 10-day cycles, the Jason-1 satellite passes our study area twice (one during ascending and the other during descending), measuring significant wave height and sea-level anomaly along-track. Fig. 2c (2d) shows the comparison between satellites observed and model simulated significant wave height (sea surface height anomaly). Both time series were temporally and spatially averaged along satellite tracks (see their positions in Fig. 3c and d). Overall, the model reproduces observed surface wave and sea level variability reasonably well. The correlation coefficients between the two time series are above 0.81 with the 95% confidence interval, lending confidence that the sediment transport and dispersion simulations were driven by a realistic hydrodynamic environment.

3.1. Seasonal hydrodynamics and sediment transport patterns

We computed monthly mean significant wave heights in August (December) and used them as the typical summer (winter) wave conditions, respectively (Fig. 3c and d). In both periods, waves are stronger in the north/northeast parts of our study domain. The mean significant wave heights in August (having a mean value of 0.88 m) are about 50% smaller than those in December (having a mean value of 1.68 m). Such a seasonal difference is a direct result of seasonal variations in the monsoon strength (Fig. 3a and b), which is much larger in winter (when NE monsoon prevails) than in summer (when SW monsoon prevails). Because the wave-driven bottom stress is proportional to the significant wave height, the coastal sediment resuspension would also be more effective in winter.

Monthly mean surface currents and suspended sediment concentration (SSC) were also calculated for August (Fig. 4a) and December (Fig. 4c). Due to a lack of in situ SSC observations, we attempted to use the Moderate Resolution Imaging Spectroradiometer (MODIS) ocean color images (Fig. 4b and d) to validate simulated surface SSC for each season. While quantitative comparisons were not possible, simulated SSC did reproduce major seasonal features of the turbidity visible in MODIS images, such as the extended turbidity plume seaward of the river mouth in summer (Fig. 4b), and the high turbidity zone confined on the inner shelf from river mouth all the way to Camau Peninsula in winter (Fig. 4d). As we mentioned earlier, this simulation only considered the sediment discharged by the Mekong River, so the SSC simulated here does not account for the contribution from resuspeneded shelf sediments.

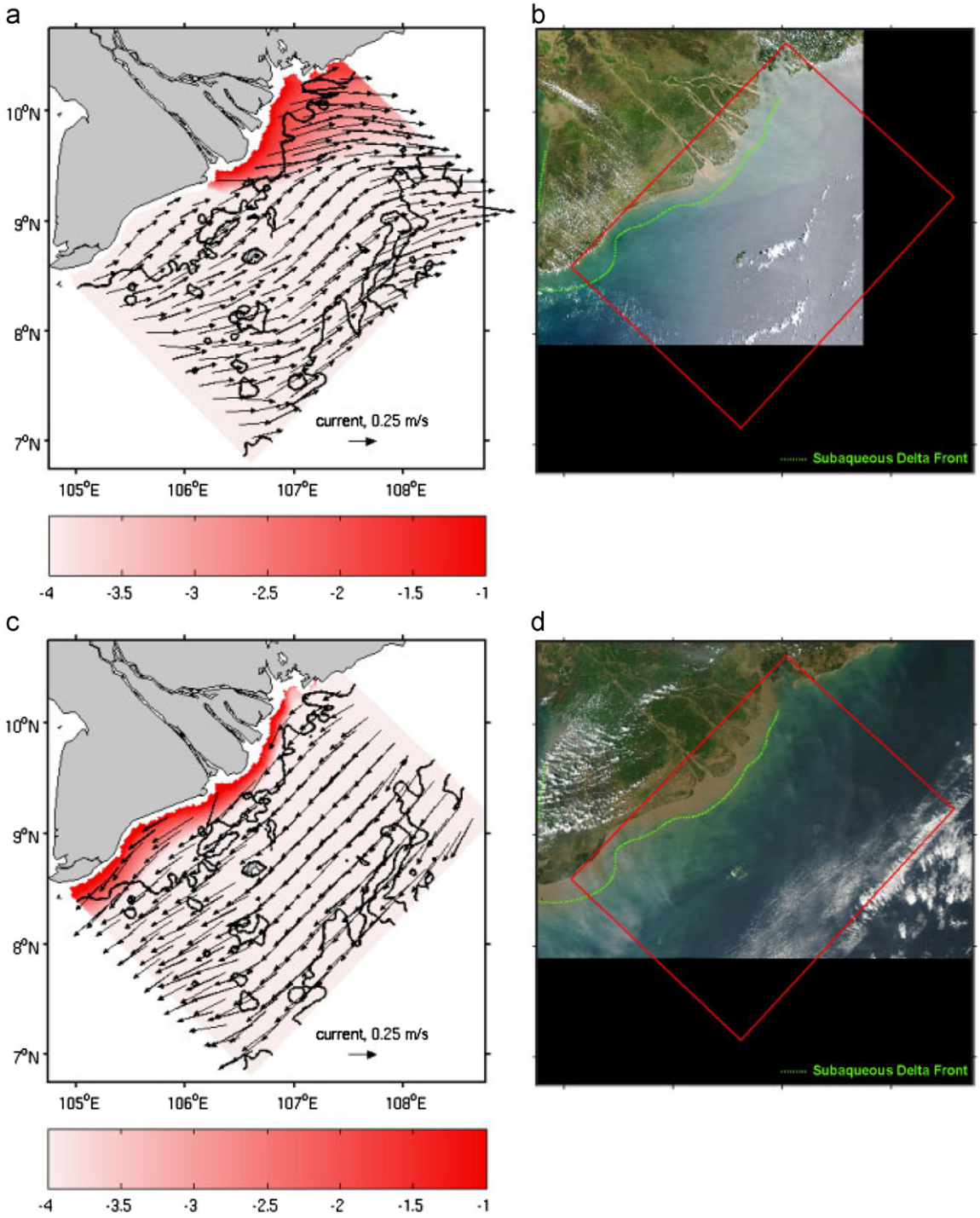

Fig. 4. Monthly mean surface suspended sediment concentration (SSC color shading) and surface current fields in (a) summer (August) and (c) winter (December), 2005. Also shown are Moderate Resolution Imaging Spectroradiometer (MODIS) images in August 2002 (b) and January 2005 (d). Simulated surface concentration (color) is shown in the log scale. (a) Surface SSC, August; Log_{10} kg/m^3, (b) MODIS image in August, (c) Surface SSC, December; Log_{10} kg/m^3 and (d) MODIZ image in January. (For interpretation of the references to color in this figure legend, the reader is referred to the web version of this article.)

Examinations of bottom currents provide additional information on seasonal differences in circulation and sediment transport. In August, upwelling favorable summer (SE) monsoon prevails. Significant onshore bottom currents are induced, helping trap a large amount of sediments along the coastline and near the river mouth (Fig. 5a). In December when downwelling favorable winter (NE) monsoon prevails, despite the low river runoff and sediment input, energetic wind and wave mixing in conjunction with southwestward coastal current transport resuspended sediment further to the southwest (Fig. 6a).

Both the transport rate for bedload and the resuspension rate for suspended sediment are determined by the bottom shear stress that are related to wave, current, and combined wave–current interaction effects. We found that the wave induced stresses are generally one order of magnitude larger than the current induced (not shown) in both August and December. However, monthly mean bed shear

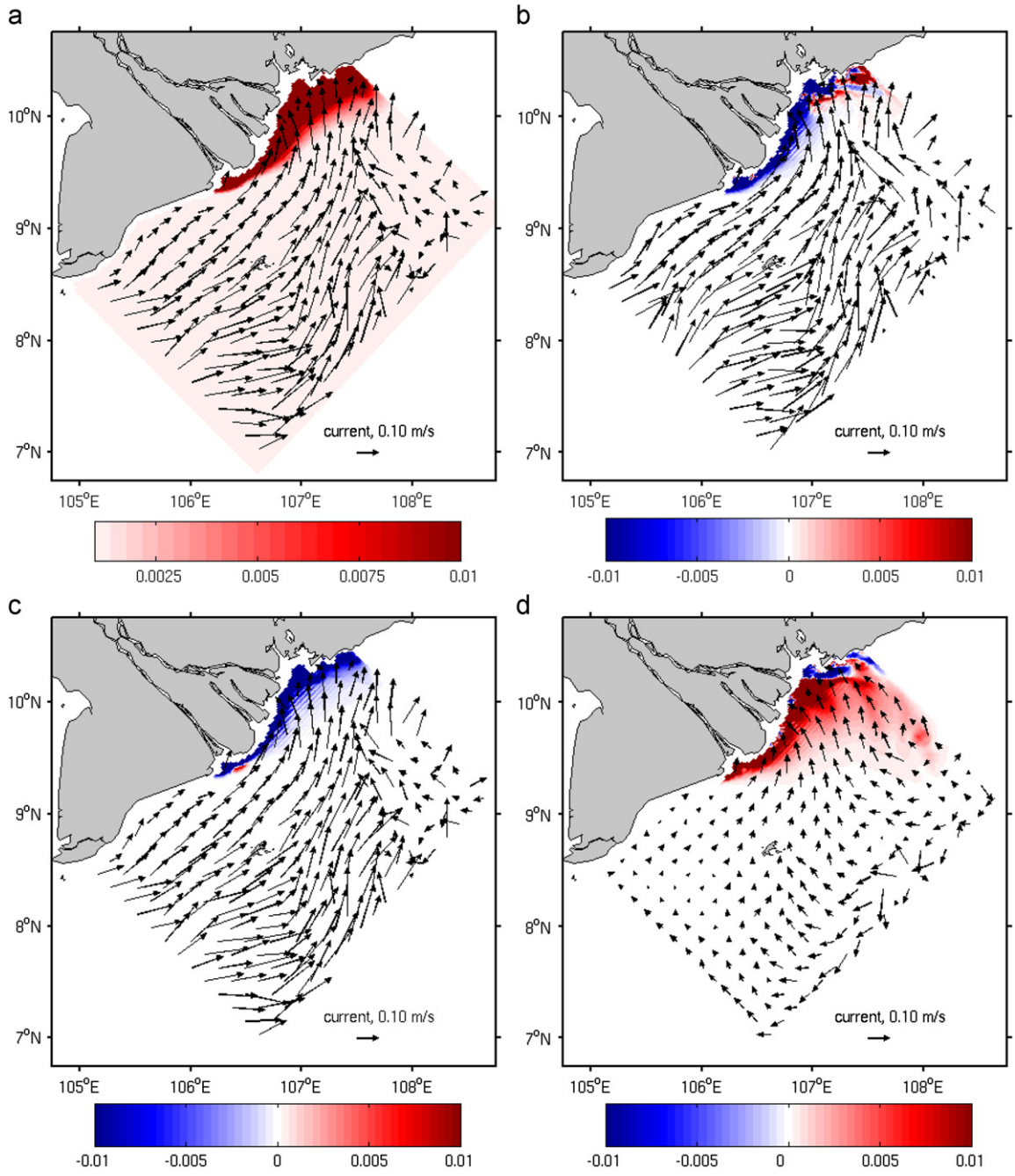

Fig. 5. Monthly mean bottom current velocities (arrows) and suspended sediment concentration (SSC) in August, 2005 calculated by Control run (a). Three model sensitivity experiments were performed. The bottom current velocity and the difference om SSC between them and the Control run are shown in (b) for NTS case (NTS minus Control), in (c) for NWS case (NWS minus Control), and in (d) for NAS case (NAS minus Control). Notice the change of color bar between (a) and (b–d). (For interpretation of the references to color in this figure legend, the reader is referred to the web version of this article.)

stresses are significantly weaker in August (Fig. 7a) than in December (Fig. 7b). The net effect is most of deposits were transported southwestward along the downdrift coast as season progresses. By the end of our 13-months simulation, i.e. Dec 31st, Mekong sediments were only seen within a short distance (<10 km) seaward of the river mouth (Fig. 8a).

3.2. *Model sensitivity experiments: relative roles of tides, waves, and ambient currents*

Three sensitivity simulations mentioned above (i.e. NTS, NWS, and NAS) were carried out. Their monthly mean fields in August and December were compared to those from the control run to highlight differences (NTS-Control, NWS-Control, NAS-Control) in SSC, bottom current, sediment transport, and dispersal pattern (Figs. 5b–d, 6b–d, 8b–d) due to the neglection of corresponding dynamics.

For NTS case in which tides was excluded, SSC in August was much less throughout the water column seaward of the river mouth (Fig. 5b). Such a pattern remains to be the case in the offshore water in December, while there is a noticeable SSC increase right at the coast (Fig. 6b), possibly due to the missing of cross-shelf transport associated with shallow water tidal residual flow. Because of this, difference in the sediment dispersal

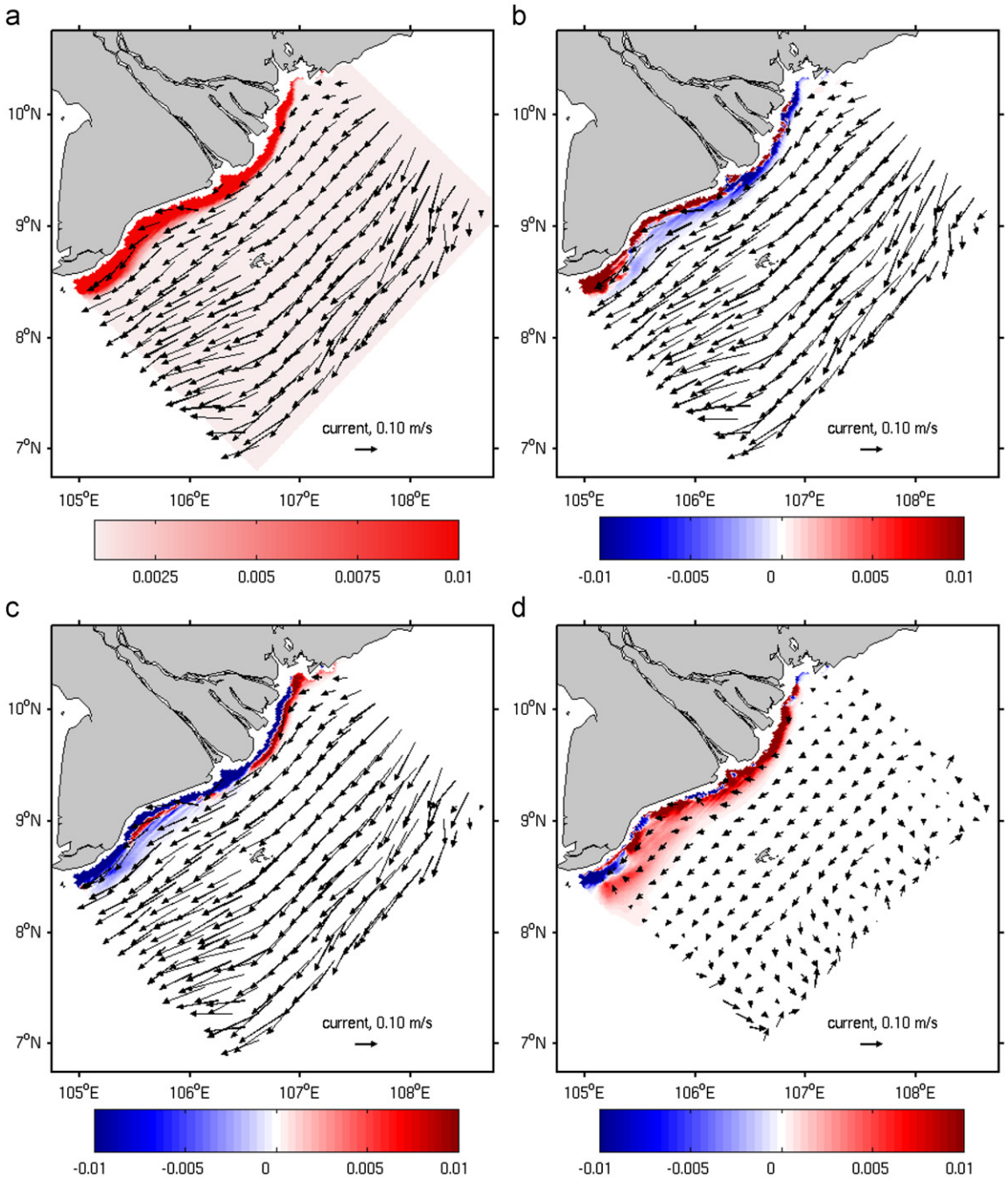

Fig. 6. Same as Fig. 5, but for December, 2005. (a) Control run, December; kg/m^3, (b) NTS-Control; kg/m^3, (c) NWS-Control; kg/m^3 and (d) NAS-Control; kg/m^3.

between the NTS and the control run by the end of the simulation (December 31) show that this is a net disposition line right along the coast (Fig. 8b).

For the NWS case, in which waves were excluded, SSC was significantly decreased throughout the water column in August (Fig. 5c), suggesting more sediment was deposited on the seafloor during this high flow season compared to the control case. The similar situation was also seen in December (Fig. 6c). Furthermore, the SSC landward of the delta front was in general smaller than those from NTS case. Without wave-induced mixing, larger sediment deposition occurred locally, leading to significant reduction in the southwestward sediment transport and downstream suspended sediment concentration (Fig. 6c). Indeed, among results of all model experiments, we see the largest local sediment depositions by December 31, which appear to spread from river mouth to deep water in cross-shelf direction (Fig. 8c).

For the NAS case, in which shelf circulation was neglected, although the sediments were continuously resuspended by the combined wave and tide mixing, the lack of mean current transport in both August (Fig. 5d) and December (Fig. 6d) lead to noticeable reduction in alongshelf sediment flux. Most of SSC changes are associated with local sediment resuspension and deposition, rather than with upstream advection process. By the end of the simulation (December 31), the difference in sediment dispersal was mainly along the coastline (Fig. 8d).

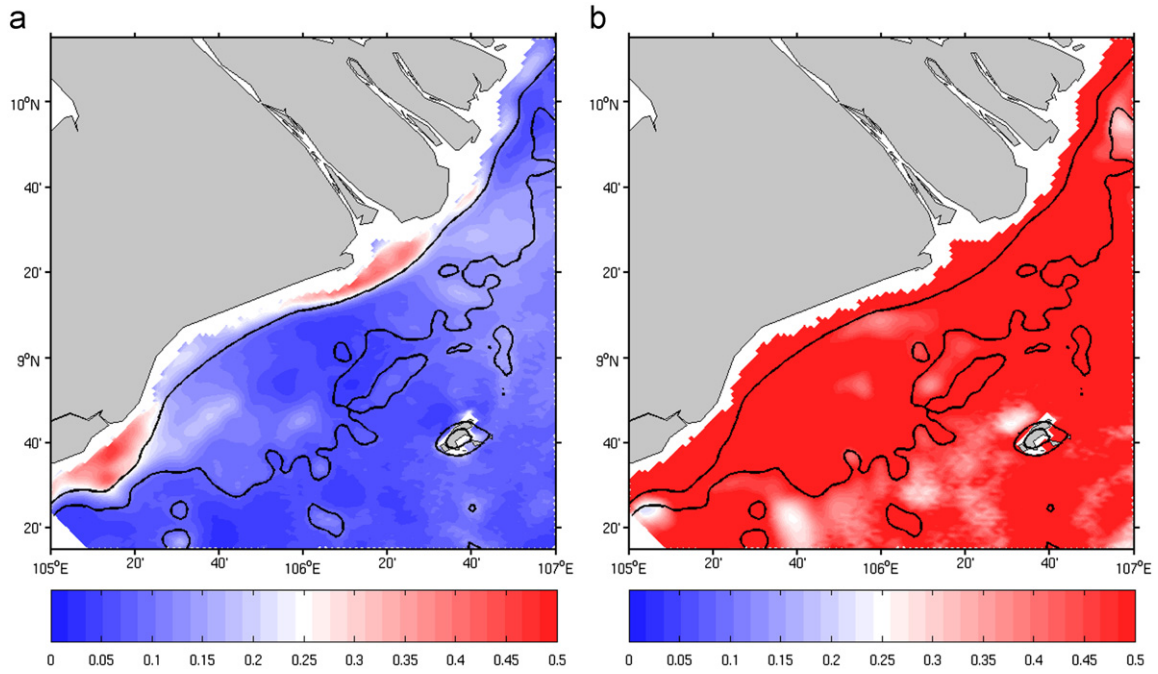

Fig. 7. Monthly mean bed shear stresses in August (a) and December (b), 2005 calculated from the control run. Depth contours in the figures are 10 m and 20 m isobaths.

4. Discussion

We simulated the Mekong shelf circulation and sediment transport and dispersal in 2005. In the following section, we intend to discuss the relevance of our results from a 13-months numerical simulation to longer time scale morphodynamics of the MRD.

The Late Holocene sediment budget estimated that $80 \pm 18\%$ of Mekong-derived sediments have been trapped on the delta front over the past 3000 yrs (Xue et al., 2010b).

Based on differences in acoustic characters and core analysis, the delta front can be further divided into four different zones, including Zone 1 for river mouth, Zone 2 for the east shore of Camau Peninsula, Zone 3 for the Camau Cape, and Zone 4 for the west shore. Zone 1 and Zone 2 are covered by the model domain used this study. We further divided Zone 1 and Zone 2 into Zone 1a and 1b and Zone 2a and 2b, where Zone 1a (Zone 2a) represent the delta front seaward of the river mouth (downdrift delta plain), and Zone 1b (Zone 2b) represent the low gradient seabed further seaward of the delta front, i.e. the pro-delta (Fig. 9). We found that in all numerical experiments in this study, by the end of the 13-months simulation, the sediment dispersal was indeed confined in the delta front. From the control run, $\sim$88.7% of the river sediment load was retained on the delta front (i.e. in Zone 1a and Zone 2a combined). From the subregional perspective, by December 31, there was 86.9% and 1.8% of fluvial sediments remain in Zone 1a and Zone 2a, respectively. The small deposition ratio in Zone 2a is a bit surprising, suggesting suspension and erosion were predominating in this area on the annual time scale.

Recall our control run was initialized with zero shelf sediment. To test model sensitivity to sediment initial condition, we also took the control run's Class 1 and 2 sediment depositions on December 31 as the alternative initial conditions of two sediment classes and performed the 2nd control simulation for 2005. In comparison with the 1st Control run solutions, we found that by the end of this simulation, the percentage of the total sediment deposition decreased from 86.9% to 80.1% in Zone 1a, and from 1.8% to 0.26% in Zone 2a. This result indicates that the model solutions are quantitatively sensitive to initial condition specifications, but qualitatively remain the same as the 1st Control run results, that is Zone 2a still receive very limited sediments from the Mekong River during the 13-month simulation period. Therefore the net Mekong-derived sediment deposition in Zone 2a inferred from the Late Holocene sediment budget estimate appears to be the result of a slow but persistent deposition process occurred over a much longer (millennial) time scale.

A general consensus has been made that the downdrift delta plain of the MRD, i.e. Zone 2a, is a result of along-shelf sediment transport (Gagliano and McIntire, 1968; Nguyen et al., 2000; Xue et al., 2010b). To examine this along-shelf transport process, we spatially averaged (within the delta front, i.e. Zone 1a and 2a combined) simulated wave orbital velocity, detided (subtidal) bottom current, and the percentage of suspended and deposited sediment from the 2nd control run. The year-long time series of each of these variables (Fig. 10) indicate that the along-shelf transport was mainly during the winter season. During this period (Oct through April), southwestward waves dominate (Fig. 10a), subtidal currents shifted the direction from northeastward (May through September) to southwestward. The strongest bottom currents occurred in January and December, with a magnitude reaching 0.1 m/s (Fig. 10b). The amount of the suspended sediment presented in the water column was also the largest in the winter season (up to 4% of fluvial inputs, Fig. 10c). Time series of percentages of suspended sediments (Fig. 10c) and deposited sediments (Fig. 10d) show a general inverse relationship (i.e., increased suspended sediment is associated with decreased deposition at seabed). Both of them exhibit large variability in winter season, corresponding nicely with seasonal variability in both wave orbital velocity and bottom current velocity.

We note that because our 13-month model hindcast simulation did not consider other relevant factors that may influence regional deposition and dispersal processes, such as sea level rise

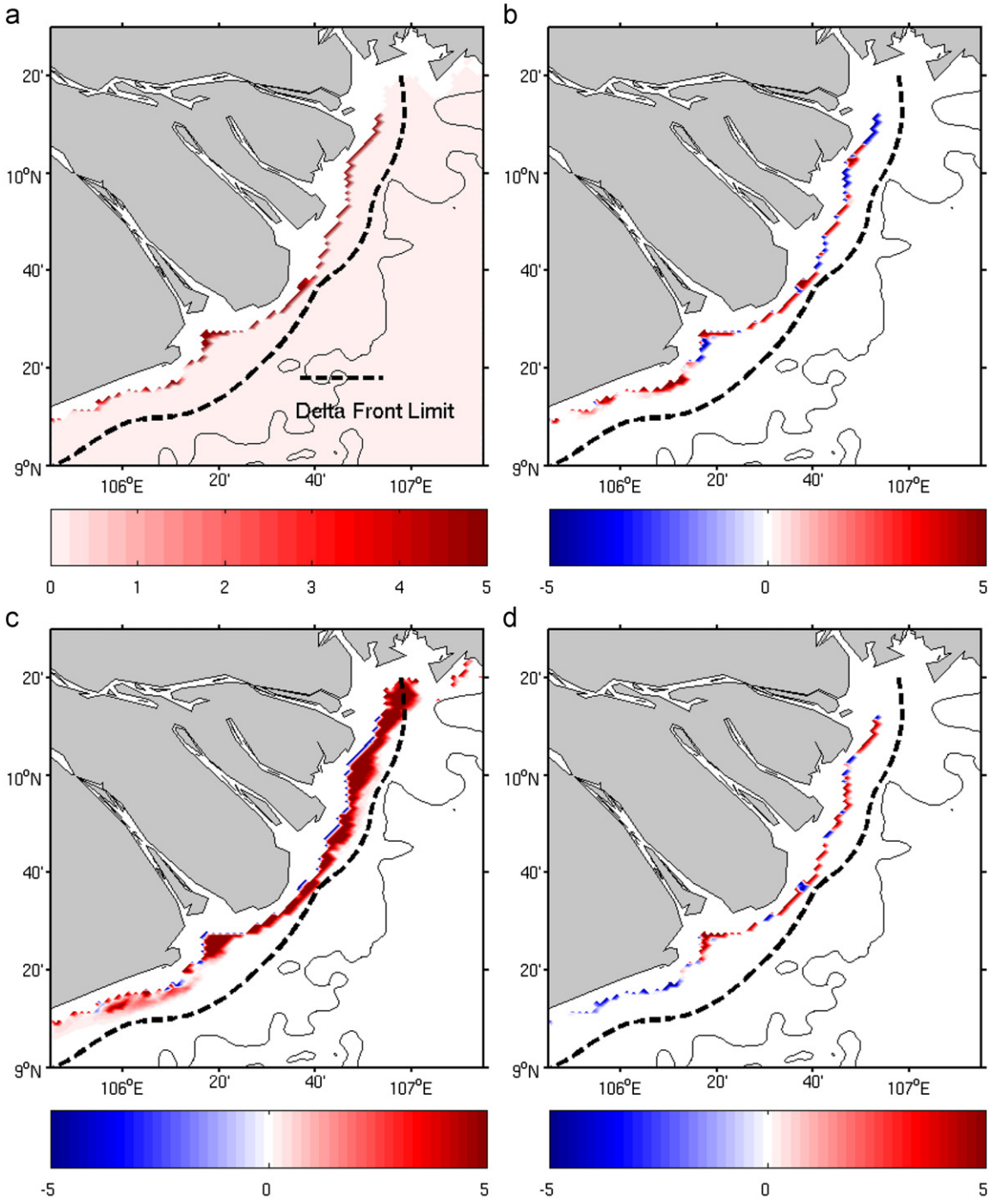

Fig. 8. Simulated Mekong-River sediment deposition on Dec 31st, 2005 by the Control run (a). Three model sensitivity experiments were performed, the deposition difference between each of them and the control run result on December 31, 2005 are shown in (b) for NTS case (NTS minus Control), in (c) for NWS case (NWS minus Control), and in (d) for NAS case (NAS minus Control). The dash line in each panel indicates the location of the delta front. Note the change of color bar between (a) and (b–d). (For interpretation of the references to color in this figure legend, the reader is referred to the web version of this article.)

and episodic but powerful typhoon activities, we cannot make a direct linkage between our simulated sediment budget on the annual time scale and early estimates of shelf-scale sediment budget and along-shelf transport based on the geological time scale. In addition, the amount of the southwestward along-shelf transported sediment in our model was very limited due to low SSC ($<4\%$, Fig. 10c) and could not represent the seasonal sediment transport mechanism in Xue et al. (2010b). We anticipate that this discrepancy may be resolved by long-term coupled modeling simulations that are initialized with more realistic bulk bed (grain size distribution, bed thickness, etc.) and account for both episodic (e.g. typhoon) and centennial/millennial time scale (e.g. sea level rise and climate change) processes.

5. Conclusions and summary

We applied a Coupled Wave–Ocean–Sediment Transport Model to simulate the Mekong shelf circulation and the transport and dispersal of Mekong-derived fine sediments in 2005. Comparisons

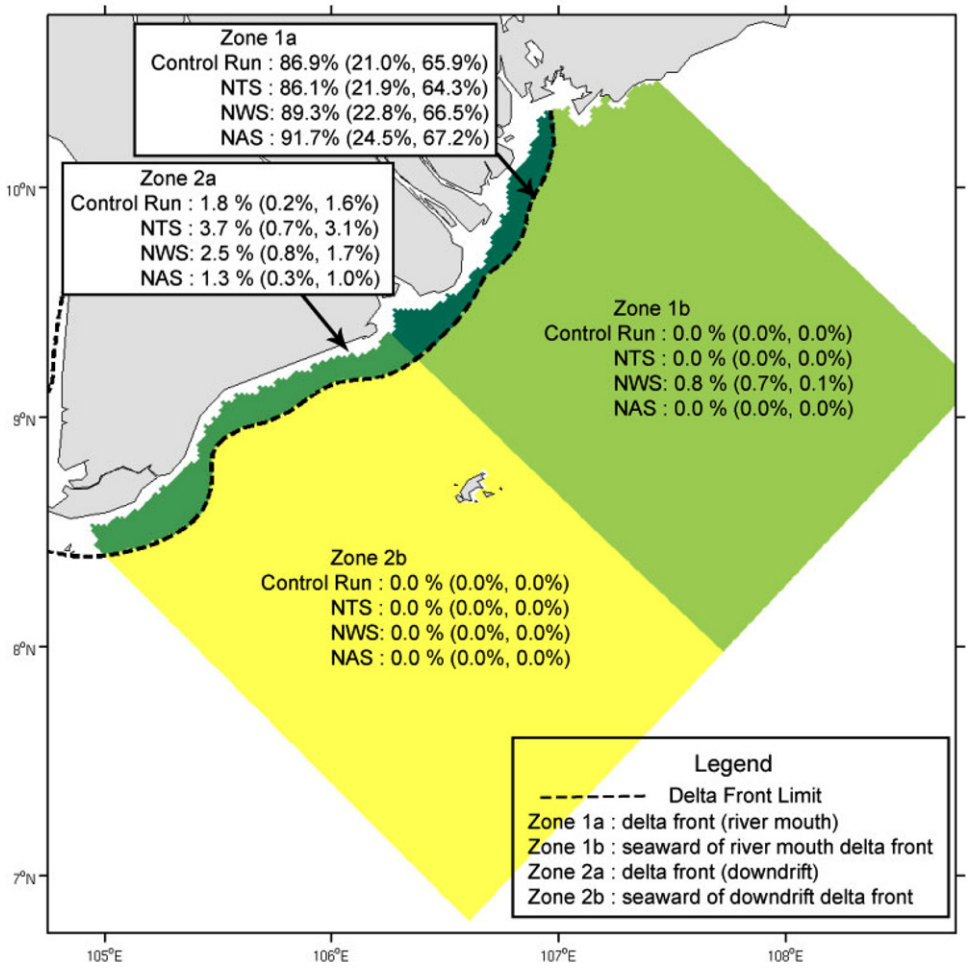

Fig. 9. A zonation map of simulated riverine sediment budget based on four model simulations (Control Run, NTS, NWS, and NAS). The dash line indicates the position of the delta front limit. Zone 1 (a and b) and Zone 2 (a and b) corresponds to the Zone 1 and Zone 2 in Xue et al. (2010b). In each case, the numbers outside and inside the parenthesis are presented in the following order: the sum of sediment Class 1 and Class 2 (sediment Class 1, sediment Class 2), showing the percentages of remaining seabed sediment on December 31, 2005.

with limited observations showed that the coupled model captured the spatial patterns and temporal variability of wave, sea level, and suspended sediment concentration reasonably well (Figs. 2 and 4). Significant seasonality in sediment transport was revealed. In summer, a large amount of fluvial sediment was delivered and deposited near the Mekong River mouth (Figs. 5a and 8a). In the following winter, strong ocean mixing and coastal current lead to resuspension and southwestward dispersal of a small fraction of previously deposited sediments (Figs. 6a, 9 and 10).

Three additional model sensitivity (with reduced physics) experiments were performed to investigate the impact of respective factors (i.e. tides, waves, and remotely forced ambient current) on the transport and dispersal of the fluvial sediment. Our sensitivity simulations indicated that the sediment dynamics of the modern MRD is jointly controlled by tides, waves, and coastal circulation in the SCS. Once tidal forcing was withdrawn, the cross-shelf transport was decreased, resulting in larger alongshelf sediments transport from Zone 1a (86.1% compared with 86.9% in control run) to Zone 2a (3.7% compared with 1.8% in control run, Fig. 9). The shear stress for resuspension was mainly induced by waves: once wave was excluded, more sediments were deposited on the delta front by the end of simulation (91.8% compared with 88.7% in control run). The southwestward alongshelf sediment transport was reduced most significantly when ambient current was withdrawn. In the NAS case 93.0% sediments were retained on the delta front by the end of the simulation, compared to 88.7% in the Control run.

While numerical modeling has a great ability to piece out different processes in a complex dynamic system, most coastal ocean modeling experiments (ours included) are relatively short simulations, focusing on time scales from days to a year, thus the long-term morphodynamical variability would still be difficult to address from these short-term numerical modeling point of views. The sediment model solutions are also sensitive to the parameterizations of sediment characteristics. Because no in-situ observations on the shelf bulk bed were available, our simulation mainly focused on the fine river sediment load and the influence on its transport by different hydrodynamic processes. The majority of our parameterization followed a Po River modeling study by Harris et al., (2008). The settling velocity of flocculated sediments is based on a previous modeling study in the estuary area (0.25 mm/s, Wolanski et al., 1998). We speculate that, as mud flocs tend to break down in salty waters, the sediments on the inner shelf could settle with a lower velocity, allowing more sediments be transported southwestward. A more comprehensive assessment of the Mekong shelf sediment budget will be possible in the future when more information on deposition thickness,

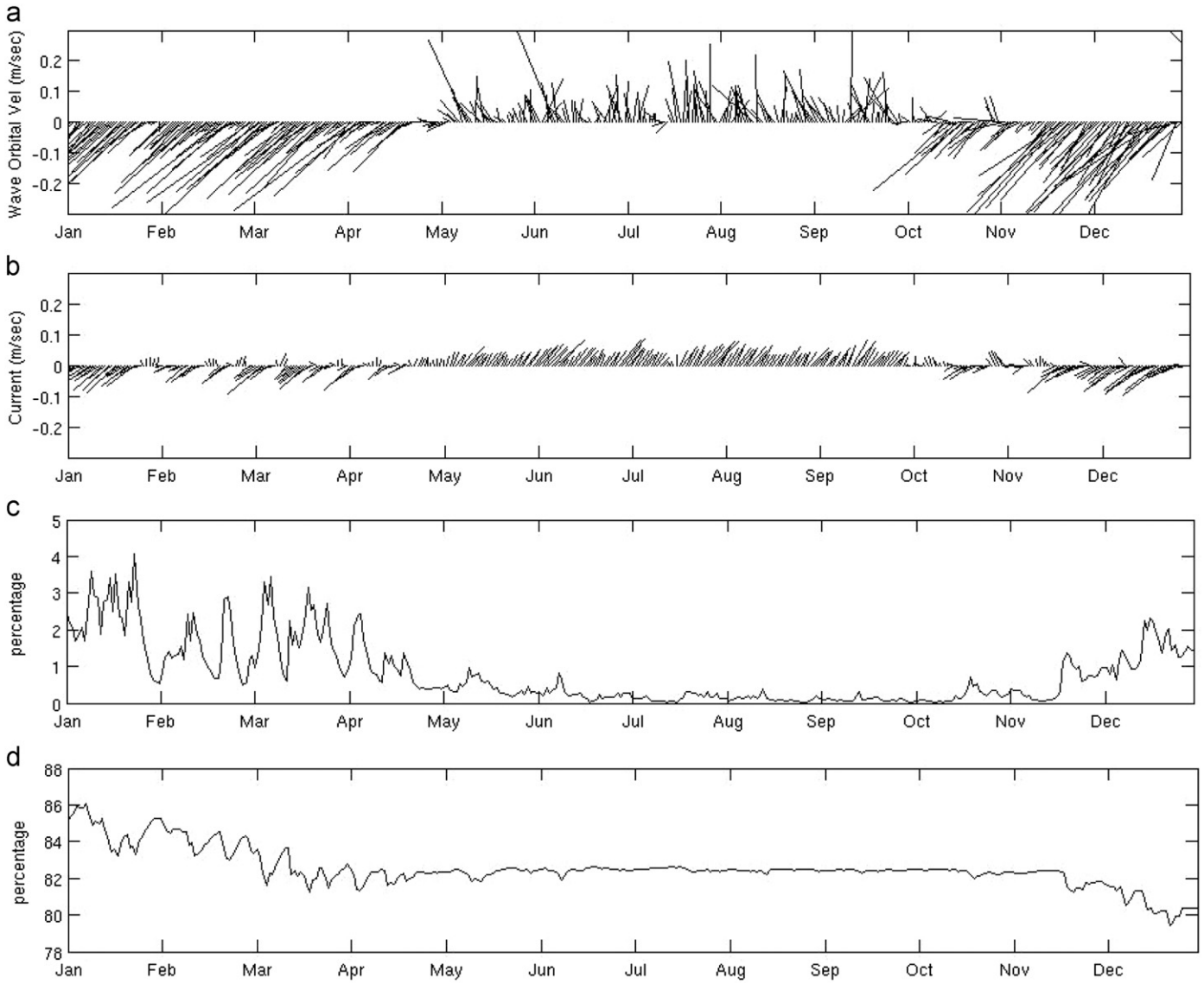

Fig. 10. Spatially averaged conditions on delta front defined in Xue et al. (2010b). (a) Wave-orbital velocities, (b) bottom current speed (detided) (c) percentage of suspended sediment concentration, and (d) percentage of sediment deposited on the seabed.

grain sizes, and critical shear stress become available. These data can be used in long-term coupled model simulations that can help us to better understand sediment transport dynamics on daily to millennial time scales.

Acknowledgment

We thank the funding supports from U.S. Geological Survey, International Office of the National Science Foundation, and Office of Naval Research. Assistance from Dr. K. Chen, Mr. Y. Li, Dr. H. Liu (North Carolina State University), Mr. Z. Yao (Ocean University of China) with the ROMS and SWAN model setup is appreciated. The MODIS satellite images and wave/sea-level data from AVISO provided crucial validation information for our numerical modeling. We also appreciate detailed and insightful comments from Dr. C.K. Harris (Virginia Institute of Marine Science) and Dr. K.H. Xu (Coastal Carolina University) as well as two anonymous reviewers.

References

Becker, J.J., Sandwell, D.T., Smith, W.H.F., Braud, J., Binder, B., Depner, J., Fabre, D., Factor, J., Ingalls, S., Kim, S.-H., Ladner, R., Marks, K., Nelson, S., Pharaoh, A., Trimmer, R., Von Rosenberg, J., Wallace, G., Weatherall, P., 2009. Global bathymetry and elevation data at 30 arc seconds resolution: SRTM30_PLUS. Marine Geodesy 32 (4), 355–371.

Bever, A.J., Harris, C.K., Sherwood, C.R., Signell, R.P., 2009. Deposition and flux of sediment from the Po River, Italy: an idealized and wintertime numerical modeling study. Marine Geology 260 (1–4), 69–80.

Booij, N., Ris, R.C., Holthuijsen, L.H., 1999. A third-generation wave model for coastal regions 1. Model description and validation. Journal of Geophysical Research 104 (C4), 7649–7666.

Chassignet, E.P., Hurlburt, H.E., Smedstad, O.M., Halliwell, G.R., Hogan, P.J., Wallcraft, A.J., Baraille, R., Bleck, R., 2007. The HYCOM (HYbrid Coordinate Ocean Model) data assimilative system. Journal of Marine Systems 65 (1–4), 60–83.

Coleman, J.M., Roberts, H.H., 1989. Deltaic coastal wetlands. Geologie en Mijnbouw 68, 1–24.

Debenay, J.-P., Luan, B.T., 2006. Foraminiferal assemblages and the confinement index as tools for assessment of saline intrusion and human impact in the Mekong Delta and neighboring areas (Vietnam). Revue de Micropaleontologie 49 (2), 74–85.

Egbert, G.D., Erofeeva, S.Y., 2002. Efficient inverse modeling of barotropic ocean tides. Journal of Atmospheric and Oceanic Technology 19, 2.

Fairall, C.W., Bradley, E.F., Rogers, D.P., Edson, J.B., Young, G.S., 1996. Bulk parameterization of air-sea fluxes for tropical ocean-global atmosphere Coupled-Ocean Atmosphere Response Experiment. Journal of Geophysical Research 101, 3747–3764.

Flather, R.A., 1976. A tidal model of the northwest European continental shelf. Memoires de la Societe Royale de Sciences de Liege 6, 141–164.

Gagliano, S.M., McIntire, W.G., 1968. Reports on the Mekong River Delta, Louisiana State University.

Gan, J., Li, H., Curchitser, E.N., Haidvogel, D.B., 2006. Modeling South China Sea circulation: response to seasonal forcing regimes. Journal of Geophysical Research 111 (C6), C06034.

Haidvogel, D.B., Arango, H., Budgell, W.P., Cornuelle, B.D., Curchitser, E., Di Lorenzo, E., Fennel, K., Geyer, W.R., Hermann, A.J., Lanerolle, L., Levin, J., McWilliams, J.C., Miller, A.J., Moore, A.M., Powell, T.M., Shchepetkin, A.F., Sherwood, C.R., Signell, R.P., Warner, J.C., Wilkin, J., 2008. Ocean forecasting in terrain-following coordinates: formulation and skill assessment of the regional ocean modeling system. Journal of Computational Physics 227 (7), 3595–3624.

Harris, C.K., Wiberg, P.L., 2001. A two-dimensional, time-dependent model of suspended sediment transport and bed reworking for continental shelves. Computers & Geosciences 27 (6), 675–690.

Harris, C.K., Sherwood, C.R., Signell, R.P., Bever, A.J., Warner, J.C., 2008. Sediment dispersal in the northwestern Adriatic Sea. Journal of Geophysical Research 113, C11S03. doi:10.1029/2006JC003868.

Hordoir, R., Polcher, J., Brun-Cottan, J.-C., Madec, G., 2006. Towards a parametrization of river discharges into ocean general circulation models: a closure through energy conservation. Climate Dynamics 31 (7–8), 891–908.

Jacob, R., Ladner, R., Ong, E., 2005. MxN communication and parallel interpolation in CCSM3 using the Model Coupling Toolkit. International Journal of High Performance Computing Applications Archive 19 (3), 293–307.

Kalnay, E., Kanamitsu, M., Kistler, R., Collins, W., Deaven, D., Gandin, L., Iredell, M., Saha, S., White, G., Wollen, J., 1996. The NCEP/NCAR 40-year reanalysis project. Bulletin of the American Meteorological Society 77, 437–470.

Kubicki, A., 2008. Large and very large subaquesous dunes on the continental shelf off southern Vietnam, South China Sea. Geo-Marine Letters 28, 229–238.

Kummu, M., Varis, O., 2007. Sediment-related impacts due to upstream reservoir trapping, the Lower Mekong River. Geomorphology 85 (3–4), 275–293.

Larson, J., Jacob, R., Ong, E., 2005. The Model Coupling Toolkit: a new Fortran90 Toolkit for building multiphysics parallel coupled models. International Journal of High Performance Computing Applications Archive 19 (3), 227–292.

Le, T.V.H., Nguyen, H.N., Wolanski, E., Tran, T.C., Haruyama, S., 2007. The combined impact on the flooding in Vietnam's Mekong River delta of local man-made structures, sea level rise, and dams upstream in the river catchment. Estuarine, Coastal and Shelf Science 71 (1–2), 110–116.

Liu, Z., Yang, H., Liu, Q., 2001. Regional dynamics of seasonal variability in the South China Sea. Journal of Physical Oceanography 31 (1), 272–284.

Liu, J.P., Xue, Z., Ross, K., Wang, H., Yang, Z.S., Li, A.C., Gao, S., 2009. Fate of sediments delivered to the sea by Asian large rivers: long-distance transport and formation of remote alongshore clinothems. SEPM-The Sedimentary Record 7 (4), 4–9.

Madsen, O.S., 1994. Spectral wave–current bottom boundary layer flows. In: Proceedings of the 24th International Conference on Coastal Engineering Research Council, Kobe, Japan, pp. 384–398.

Marchesiello, P., McWilliams, J.C., Shchepetkin, A., 2001. Open boundary conditions for long-term integration of regional oceanic models. Ocean Modelling 3 (1–2), 1–20.

Mellor, G.L., Yamada, T., 1982. Developement of a turbulence closure model for geophysical fluid problems. Reviews of Geophysics and Space Physics 20, 851–875.

Milliman, J.D., Syvitski, J.P.M., 1992. Geomorphic/tectonic control of sediment discharge to the ocean: the importance of small mountainous rivers. Journal of Geology 100, 525–544.

Nguyen, L.V., Ta, T.K.O., Tateishi, M., 2000. Late Holocene depositional environments and coastal evolution of the Mekong River Delta, Southern Vietnam. Journal of Asian Earth Sciences 18 (4), 427–439.

Saito, Y., 2000. Deltas in Southeast and East Asia: their evolution and current problems. In: Mimura, N., Yokoki H (Eds), Proceedings of APN/SURVAS/LOICZ Joint Conference on Coastal Impact of Climate Change and Adaption in the Asia-Pacific Region, Kobe, Japan, pp. 185–191.

Shaw, P.-T., Chao, S.-Y., Fu, L.-L., 1999. Sea surface height variations in the South China Sea from satellite altimetry. Oceanologica Acta 22 (1), 1–17.

Shchepetkin, A.F., McWilliams, J.C., 2005. The Regional Ocean Modeling System (ROMS): a split-explicit, free-surface, topography-following coordinates ocean model. Ocean Modelling 9, 347–404.

Shchepetkin, A.F., McWilliams, J.C., 2009. Correction and commentary for "Ocean forecasting in terrain-following coordinates: formulation and skill assessment of the regional ocean modeling system" by Haidvogel et al. Journal of Computational Physics 227, 3595–3624.Shchepetkin, A.F., McWilliams, J.C., 2009. Correction and commentary for ocean forecasting in terrain-following coordinates: formulation and skill assessment of the regional ocean modeling system by Haidvogel et al. Journal of Computational Physics 228, 8985–9000.

Skamarock, W.C., Klemp, J.B., Dudhia, J., Gill, D.O., Barker, D.M., Wang, W., Powers, J.G., 2005. A Description of the Advanced Research WRF Version 2. NCAR Technical Note: NCAR/TN-468+STR.

Stanley, D.J., Warne, A.G., 1994. Worldwide initiation of Holocene Marine Deltas by deceleration of sea-level rise. Science 265 (5169), 228–231.

Styles, R., Glenn, S.M., 2000. Modeling stratified wave and current bottom boundary layers on the continental shelf. Journal of Geophysical Research 105 (C10), 2000.

Syvitski, J.P.M., Vorosmarty, C.J., Kettner, A.J., Green, P., 2005. Impact of humans on the flux of terrestrial sediment to the global coastal ocean. Science 308 (5720), 376–380.

Syvitski, J.P.M., Kettner, A.J., Overeem, I., Hutton, E.W.H., Hannon, M.T., Brakenridge, G.R., Day, J., Vorosmarty, C., Saito, Y., Giosan, L., Nicholls, R.J., 2009. Sinking deltas due to human activities. Nature Geoscience 2 (10), 681–686.

Ta, T.K.O., Nguyen, V.L., Tateishi, M., Kobayashi, I., Saito, Y., Nakamura, T., 2002a. Sediment facies and Late Holocene progradation of the Mekong River Delta in Bentre Province, southern Vietnam: an example of evolution from a tide-dominated to a tide- and wave-dominated delta. Sedimentary Geology 152 (3–4), 313–325.

Ta, T.K.O., Nguyen, V.L., Tateishi, M., Kobayashi, I., Tanabe, S., Saito, Y., 2002b. Holocene delta evolution and sediment discharge of the Mekong River, southern Vietnam. Quaternary Science Reviews 21 (16–17), 1807–1819.

Tamura, T., Saito, Y., Sieng, S., Ben, B., Kong, M., Sim, I., Choup, S., Akiba, F., 2009. Initiation of the Mekong River delta at 8 ka: evidence from the sedimentary succession in the Cambodian lowland. Quaternary Science Reviews 28 (3–4), 327–344.

Tolman, H., 2002. User Manual and System Documentation of WAVEWATCH-III Version 2.22, US Department of Commerce, NOAA.

Traykovski, P., Wiberg, P.L., Geyer, W.R., 2007. Observations and modeling of wave-supported sediment gravity flows on the Po prodelta and comparison to prior observations from the Eel shelf. Continental Shelf Research 27 (3–4), 375–399.

Wang, G., Chen, D., Su, J., 2006. Generation and life cycle of the dipole in the South China Sea summer circulation. Journal of Geophysical Research 111 (C6), C06002.

Warner, J.C., Sherwood, C.R., Signell, R.P., Harris, C.K., Arango, H.G., 2008. Development of a three-dimensional, regional, coupled wave, current, and sediment-transport model. Computers & Geosciences 34 (10), 1284–1306.

Warner, J.C., Armstrong, B., He, R., Zambon, J.B., 2010. Development of a Coupled Ocean–Atmosphere–Wave–Sediment Transport (COAWST) modeling system. Ocean Modeling 35 (3), 230–244.

Wiberg, P.L., Harris, C.K., 1994. Ripple geometry in wave-dominated environments. Journal of Geophysical Research 99 (C1), 775–789.

Wolanski, E., Ngoc Huan, N., Trong Dao, L., Huu Nhan, N., Ngoc Thuy, N., 1996. Fine-sediment dynamics in the Mekong River Estuary, Vietnam. Estuarine, Coastal and Shelf Science 43 (5), 565–582.

Wolanski, E., Nguyen, H.N., Spagnol, S., 1998. Sediment dynamics during low flow conditions in the Mekong River Estuary, Vietnam. Journal of Coastal Research 14, 472–482.

Xue, Z., Liu, J.P., Ge, Q., 2010a. Changes in hydrology and sediment delivery of the Mekong River in the last 50 years: connection to damming, monsoon, and ENSO. Earth Surface Processes and Landforms. doi:10.1002/esp.2036.

Xue, Z., Liu, J.P., DeMaster, D., Nguyen, V.L., Ta, T.K.O., 2010b. Late Holocene evolution of the Mekong subaqueous delta, southern Vietnam. Marine Geology 269 (1–2), 46–60.

Zu, T., Gan, J., Erofeeva, S.Y., 2008. Numerical study of the tide and tidal dynamics in the South China Sea. Deep-Sea Research I 55, 137–154.